Full- and Partial Admission Performance of the Simplex Turbine

Daniel J. Dorney*, Lisa W. Griffin§
NASA Marshall Space Flight Center
Applied Fluid Dynamics Analysis Group
MSFC, AL 35812

Douglas L. Sondak#
Boston University
Office of Information Technology
Boston, MA 02215

ABSTRACT

The turbines used in rocket-engine applications are often partial-admission turbines, meaning that the flow enters the rotor over only a portion of the annulus. These turbines have been traditionally analyzed, however, assuming full-admission characteristics. This assumption enables the simulation of only a portion of the 360-degree annulus, with periodic boundary conditions applied in the circumferential direction. While this traditional approach to the simulating the flow in partial-admission turbines significantly reduces the computational requirements, the accuracy of the solutions has rarely been evaluated. In the current investigation, both full- and partial-admission three-dimensional unsteady Navier-Stokes simulations were performed for a partial-admission turbine designed and tested at NASA Marshall Space Flight Center. The results indicate that the partial-admission nature of the turbine must be included in simulations to properly predict the performance and flow unsteadiness of the turbine.

NOMENCLATURE

M	- Mach number
P	- Static pressure
Pt	- Total Pressure
Tt	- Total temperature
W	- Work
α	- Absolute circumferential angle
β	- Relative circumferential angle
η	- Total-to-total efficiency

INTRODUCTION

Partial-admission turbines are used in many high-speed applications, especially in rocket engines. In a partial-admission environment the flow enters the turbine rotor over only a portion of the complete annulus. Thus, the turbine rotors periodically pass through flowing regions and regions of no flow. The turbine airfoils, therefore, operate in an unsteady flow environment that is strongly dependent on the circumferential location of the airfoils. Historically, partial-admission turbines have been analyzed using full-admission flow assumptions, namely that the flow

* Aerospace Engineer, Associate Fellow AIAA.
§ Team Leader, Senior Member AIAA.
# Senior Scientific Programmer, Senior Member AIAA.

is periodic and that only a portion of the annulus need be simulated. The impact of this assumption on the design and predicted performance of partial-admission turbines has not been thoroughly investigated. Some theoretical and experimental studies of partial–admission turbines include the works of Horlock [1], Boulbin et al. [2], and Huzel and Huang [3].

The objective of the current study is to characterize the unsteady and time-averaged flow fields in a partial-admission turbine by performing full- and partial-admission simulations of the Simplex turbine. This will help to assess the inaccuracies due to the full-admission assumption commonly used for design purposes. The Simplex turbine was designed and tested at NASA Marshall Space Flight Center to study the use of composite materials in high-speed turbine geometries. The computational simulations were performed using a three-dimensional time-dependent Navier-Stokes analysis. The numerical results have been compared with limited experimental data.

NUMERICAL PROCEDURE

The governing equations considered in this study are the time-dependent, three-dimensional Reynolds-averaged Navier-Stokes equations. The algorithm consists of a time-marching, implicit, finite-difference scheme. The procedure is third-order spatially accurate and second-order temporally accurate. The inviscid fluxes are discretized according to the scheme developed by Roe [4]. The viscous fluxes are calculated using .standard central differences. An approximate-factorization technique is used to compute the time rate changes in the primary variables. Newton sub-iterations are used at each global time step to increase stability and reduce linearization errors. For all cases investigated in this study, one Newton sub-iteration was performed at each time step. The turbulent viscosity is calculated using the two-layer Baldwin-Lomax algebraic turbulence model [5]. Message Passing Interface (MPI) and OpenMP application program interfaces (API's) are used for parallel processing to reduce the computation time.

The Navier-Stokes analysis uses O- and H-type zonal grids to discretize the flow field and facilitate relative motion of the rotating components (see Fig. 1). The O-grids are body-fitted to the surfaces of the airfoils and generated using an elliptic equation solution procedure. They are used to properly resolve the viscous flow in the blade passages and to easily apply the algebraic turbulence model. The algebraically generated H-grids are used to discretize the remainder of the flow field, including the nozzles.

The computational analysis has been validated on several supersonic turbine geometries (e.g., Refs. 6 and 7).

BOUNDARY CONDITIONS

The theory of characteristics is used to determine the boundary conditions at the inlet and exit of the computational domain. The total pressure, total temperature, and the circumferential and radial flow angles are specified as a function of the radius. The upstream running Riemann invariant is extrapolated from the interior of the computational domain.

At outflow boundary the circumferential and radial flow angles, total pressure, and the total temperature are extrapolated from the interior of the computational domain. The total-to-static pressure ratio is specified at mid-span of the computational exit and the pressure at all other radial locations at the exit is obtained by integrating the equation for radial equilibrium. Periodicity is enforced along the outer boundaries of the H-grids in the circumferential direction.

At solid surfaces the relative velocity is set to zero, the normal derivative of the pressure is set to zero, and the surfaces are assumed to be adiabatic.

GEOMETRY AND FLOW CONDITIONS

The single-stage supersonic turbine, called Simplex, includes straight centerline nozzles and was designed and tested at NASA Marshall Space Flight Center. The turbine was tested with both metallic and composite rotor airfoils, and the time-averaged total temperatures and total pressures were recorded at several locations in the rig.

The Simplex turbine geometry includes 6 straight centerline nozzles, flowing over half the annulus, and 95 rotors. In the full-admission simulation it was assumed the turbine contained 12 nozzles (i.e., equally-spaced flowing nozzles around the annulus) and 96 rotors, with the rotors being scaled by the factor of 95/96. A 1-nozzle/8-rotor model was then simulated. In the partial-admission simulation the actual turbine geometry of 6 flowing nozzles (covering half the annulus) and 95 rotors was simulated. The spanwise sectional grids for the rotors in both simulations contained approximately 5,000 grid points. The full-admission simulations utilized 31 spanwise planes, while the partial-admission utilized 15 spanwise planes. The use of 15 spanwise planes

was deemed acceptable based on the length scales of the unsteadiness associated with the nozzles. Each straight centerline nozzle was modeled with approximately 270,000 grid points. Thus, a total of approximately 1.3 million grid points were used in the full-admission simulation and approximately 7.1 million grid points were used in the partial-admission simulation. The computational grids for the nozzles and rotors are shown in Fig. 1.

The flow enters the nozzles at a Mach number of approximately M=0.25 and a total pressure of P_t=801 psia. The peak Mach number in the nozzle is approximately M=2.80. The total-to-static pressure ratio across the complete turbine is approximately 15. The operating fluid in the rig tests was gaseous nitrogen, while the operating fluid in the engine and current simulations is oxygen.

Both simulations were run for more than one complete rotor revolution. The simulations were performed on 17 to 38 450-MHz processors of an SGI Origin2000 located at NASA Ames Research Center. The simulations required approximately $3x10^{-6}$ sec/grid point/iter CPU time per processor on 38 processors.

RESULTS

Figures 2 and 3 display Mach number contours in one nozzle from the full-admission and partial-admission simulations, respectively. The figures represent the same relative position between the nozzle and the rotors. In the full-admission simulation the rotor flow field exerts a back-pressuring effect on the nozzle, causing the nozzle exit flow to develop a subsonic core (see Fig. 2). This is a direct consequence of assuming flowing nozzles around the complete annulus in conjunction with the known experimental (partial-admission) exit boundary conditions.

One view of instantaneous Mach contours for the entire turbine (nozzles and rotors) in the full-admission and partial-admission simulations are shown in Figs. 4 and 5, respectively. In the partial-admission simulation the thick wakes associated with the solid wall regions between adjacent nozzles are clearly visible. The low-speed flow regions outside the influence of the nozzles are also evident near the bottom of Fig. 5. In the full-admission simulation the subsonic flow region at the nozzle exit causes a higher static pressure entering the rotor. Therefore, there is a greater acceleration in the rotor to achieve the prescribed exit pressure. The relative Mach number in the full-admission simulation remains supersonic to the turbine exit.

A second perspective of the instantaneous Mach contours is shown in Figs. 6 and 7. The non-uniform flow across the nozzle exit is observed in Fig 6, followed by high-speed flow throughout the rotor. This phenomenon washes out the wakes created by the solid wall region between adjacent nozzles. The partial-admission solution contains a large region of low speed flow outside the influence of the flowing nozzles, except for the flow carried along in blade passages by the rotating blades.

Tables 1 and 2 contain the mass- and time-averaged flow quantities at the inlet and exit of the nozzles and rotors, respectively. The flow quantities at the nozzle inlet are similar, except the mass flow in the full-admission simulation is twice that of the partial-admission simulation. The average Mach number and total pressure are higher at the nozzle exit in the partial-admission simulation. As noted earlier, the differences are caused by the rotor exerting a strong back pressure effect in the full-admission simulation. The large differences in the rotor inlet and exit conditions are the result of including the region of low flow outside the influence of the flowing nozzles in the averaging process for the partial-admission simulation. Confining the averaging process to the regions of the annulus influenced by the flowing nozzles results in closer agreement of the flow quantities, but disregards the important partial-admission flow phenomena. The efficiency and work in the full-admission simulation are, as expected, greater than in the partial-admission simulation. In the experiments the determination of the efficiency was based in part on three probes located at different circumferential locations at the exit of the rotor. Two of the probes were located within the influence of the flowing nozzles, while one was in the low flow region. Thus, the experimental efficiency of 60.5% should be biased towards the value predicted in the full-admission simulation. Indeed, the experimental efficiency is bracketed by the predicted partial-admission value of 50.4% and full-admission value of 63.3%. The discrepancies between the experimental and predicted efficiencies are likely the result of many sources, including: a) the tests were run in nitrogen and the simulations were run for oxygen, b) the limitations of the computational grid density, and c) only a small number of data acquisition locations were used in the experiments because the focus of the program was the turbine materials.

Figure 8 displays unsteady pressure envelopes at three spanwise locations from the full-admission

simulation. Figure 9 displays similar envelopes from the partial-admission simulation when the blades are moving through the half of the annulus with the flowing nozzles, while Fig. 10 displays the envelopes from the partial-admission simulation when the blades traverse both the flowing and non-flowing regions. Both simulations exhibit relatively constant loading across the span, while the full-admission simulation indicates significantly more unsteadiness. It is worth noting that the rotor does not become completely unloaded as it moves through the region outside of the flowing nozzles.

Unsteady pressure traces at various locations along the midspan of the rotor are shown for the full-admission simulations in Fig. 11. Figures 12 and 13 show traces from the partial-admission simulation corresponding to the blades moving through the flowing portion (Fig. 12) and both the flowing/non-flowing portions of the annulus (Fig. 13). Figures 14 to 16 contain the Fourier decompositions corresponding to the pressure traces in Figs. 11-13, respectively. In the full-annulus simulation the dominant unsteadiness on the suction surface is the nozzle-passing frequency (approximately 5000 Hz), while the pressure surface experiences significant unsteadiness at both the fundamental and twice the nozzle-passing frequency. The harmonic content is generated by two sources: a) the pressure variations across the nozzle exit shown in Fig. 2, and b) the reflection of the rotor bow shock off the solid region between adjacent nozzles. The dominant unsteadiness when the rotors are in the nozzle jets in the partial-admission simulation is at the nozzle-passing frequency, although a moderate amount of unsteadiness is also present at twice the nozzle-passing frequency. As expected, when the rotor traverses both flowing and non-flowing regions in the partial-admission simulation the higher harmonic content (especially that associated with rotor bow shock reflection) is reduced and more low-frequency content is observed. It is interesting to note that even when the rotors are outside the flowing nozzle regions they still experience unsteadiness associated with the nozzle-passing frequency, albeit at a lower level. This implies that the interactions between the rotors and nozzles drive the unsteadiness of the entire system, not just the flowing portion of the annulus.

The unsteady axial, radial and tangential forces on the rotors from the two simulations are shown in Fig. 17. The overall levels of the forces are similar in both simulations. The forces in the full-admission simulation exhibit two peaks as the rotors move through the nozzle flow. These peaks are generated by the presence of the subsonic flow over a portion of the nozzle exit (shown in Fig. 2). As expected the results of the partial-admission simulation indicate that the rotors windmill when outside the region of the flowing nozzles.

CONCLUSIONS

Full- and partial-admission unsteady three-dimensional simulations have been performed for a partial-admission supersonic turbine designed and tested at NASA Marshall Space Flight Center. The results of the partial-admission simulation show favorable agreement with the design Mach numbers and velocity triangles of the nozzles and rotors. The results of the full-admission simulation exhibit fair agreement with the experimental efficiency, which was determined by probes biased towards the flowing regions of the annulus. The full- and partial-admissions simulations gave significantly different nozzle exit flow profiles and rotor velocity fields. The partial-admission rotor exit relative Mach number is subsonic, as is the design intent. In the full-admission simulation, however, the relative Mach number remains supersonic to the rotor exit. The differences between the results of the two simulations underscore the need for modeling the complete annulus for partial-admission geometries.

ACKNOWLEDGEMENTS

The authors would like to acknowledge the use of the supercomputer facilities at NASA Ames Research Center, and especially thank Mr. Chuck Niggley and Mr. Herbert Yeung for their assistance. The authors would also like to thank Mr. Matt Marsh of NASA/MSFC for his help in interpreting the experimental data.

REFERENCES

1. Horlock, J. H., *Axial Flow Turbines,* Chapter 7, Butterworth, London, 1966.

2. Boulbin, F., Penneron, N., Kermarec, J. and Pluviose, M., "Turbine Blade Forces Due to Partial Admission," Revue Francaise de Mecanique, 1992-1993.

3. Huzel, D. K. and Huang, D. H., *Design of Liquid-Propellant Rocket Engines,* AIAA Progress in Astronautics and Aeronautics, Vol. 147, A. Richard Seebass Editor-in Chief, Chapter 6, 1992.

4. Roe, P. L., ``Approximate Riemann Solvers, Parameter Vectors, and Difference Schemes,'' *Journal of Computational Physics*, Vol. 43, 1981, pp. 357-372.

5. Baldwin, B. S., and Lomax, H., ``Thin Layer Approximation and Algebraic Model for Separated Turbulent Flow,'' AIAA Paper 78-257, Huntsville, AL, January, 1978.

6. Griffin, L. W. and Dorney, D. J., ``Simulations of the Unsteady Flow Through the Fastrac Supersonic Turbine,'' *ASME Journal of Turbomachinery*, Vol. 122, No. 2, April, 2000, pp. 225-233.

7. Dorney, D. J., Griffin, L. W., and Huber, F., ``A Study of the Effects of Tip Clearance in a Supersonic Turbine,'' *ASME Journal of Turbomachinery*, Vol. 122, No. 4, October, 2000, pp. 674-673.

Variable	Inlet Full Admission	Inlet Partial Admission	Exit Full Admission	Exit Partial Admission
M	0.274	0.254	1.06	1.39
α (deg)	0	0	-73.4	-74.1
P (psia)	75.4	76.1	78.9	78.6
Pt (psia)	801	801	316	434
Tt (R)	799	799	789	786
Mdot (lbm/sec)	16.5	8.3	16.6	8.3

Table 1. Nozzle inlet and exit flow quantities.

Variable	Inlet Full Admission	Inlet Partial Admission	Exit Full Admission	Exit Partial Admission
M (abs)	0.925	0.874	0.664	0.410
M (rel)	0.612	0.737	1.183	0.769
α (deg)	-56.7	-68.5	28.2	2.70
β (deg)	-22.8	26.8	61.2	71.1
P (psia)	114.	72.8	51.1	51.1
Pt (abs psia)	280	208	70.5	61.8
Pt (rel psia)	157	116	126	89.6
Tt (abs R)	767	757	540	585
Tt (rel R)	681	710	639	652
Mdot (lbm/sec)	16.6	8.3	16.7	8.3
$\eta_{t\text{-}t}$	--	--	63.3	50.4
W (BTU/lbm)			57.3	44.0

Table 2. Rotor inlet and exit flow quantities.

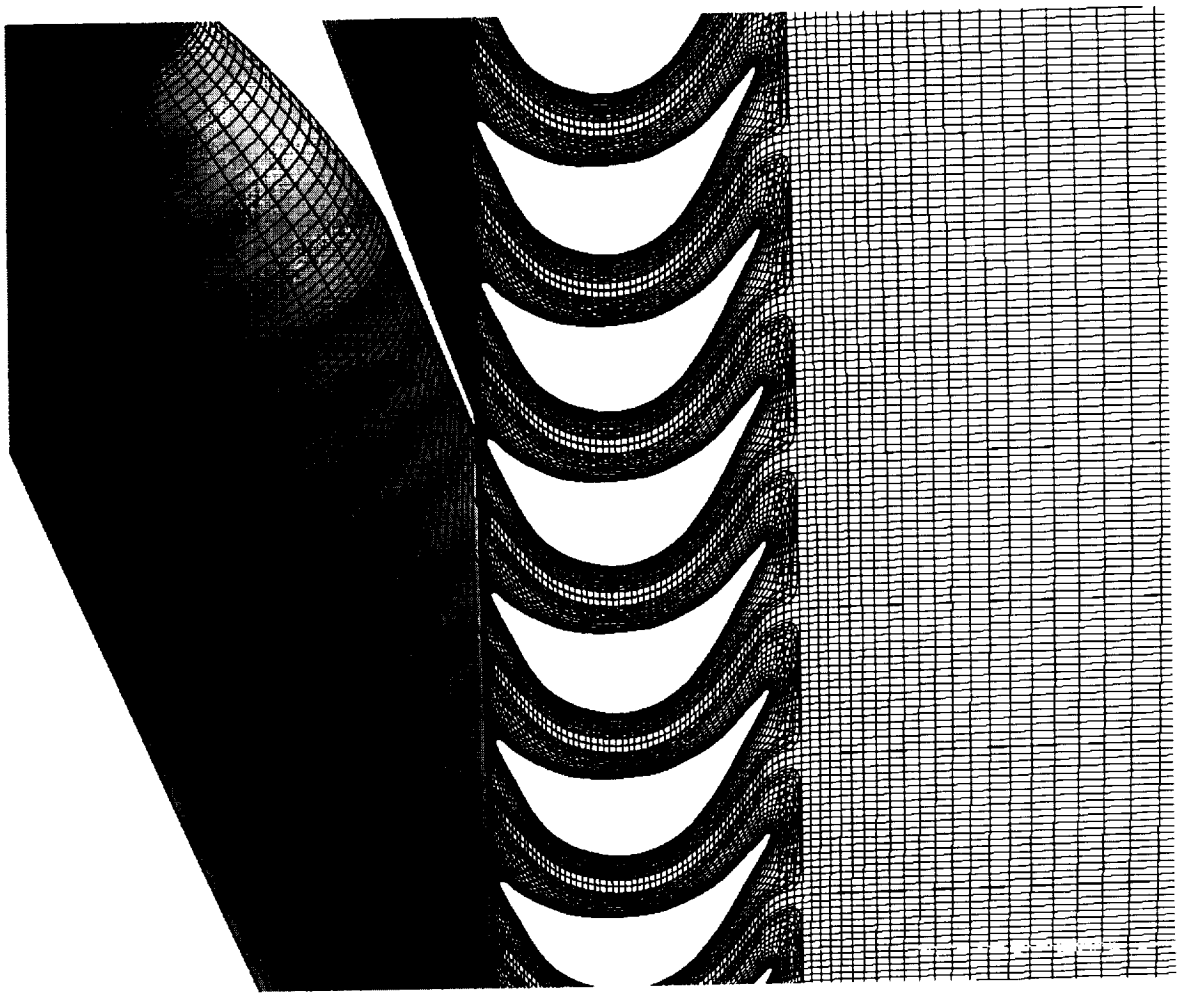

Figure 1. Computational grids for the nozzles and rotors.

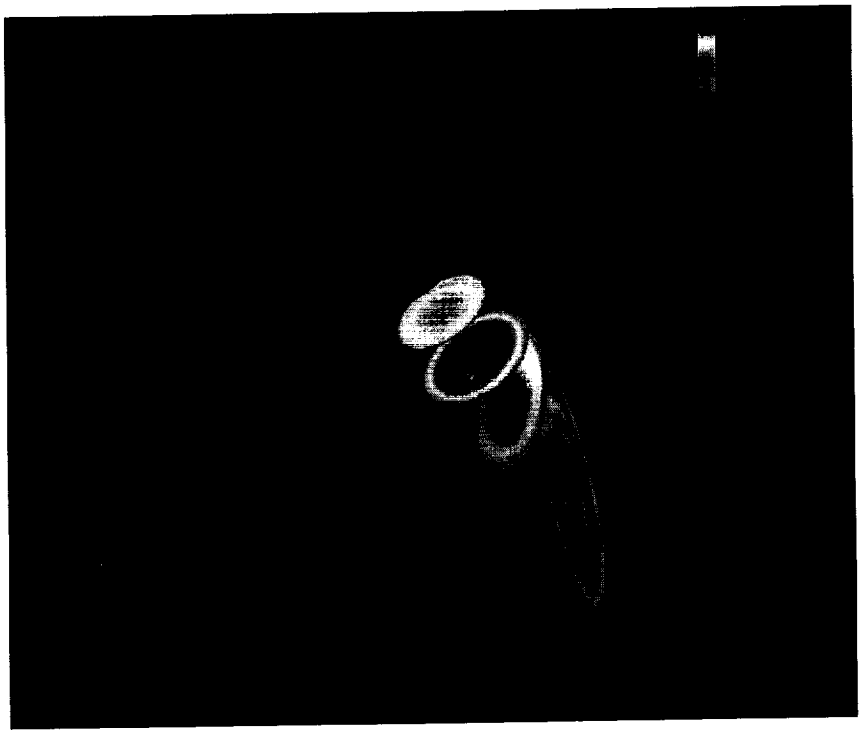

Figure 2. Instantaneous Mach contours - nozzle - full admission.

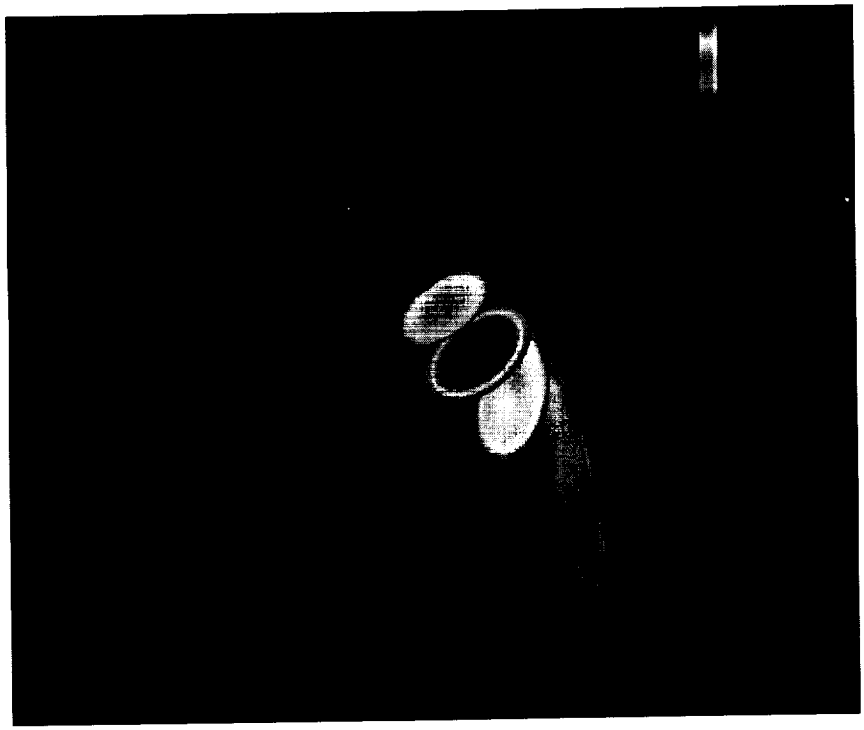

Figure 3. Instantaneous Mach contours - nozzle - partial admission.

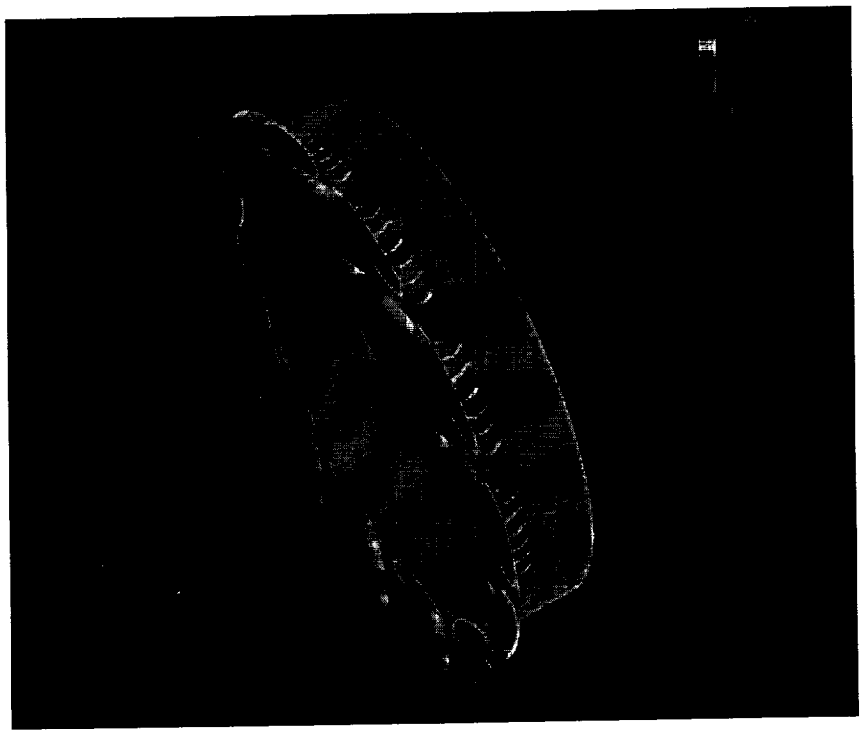

Figure 4. Instantaneous Mach contours - upstream view - full admission.

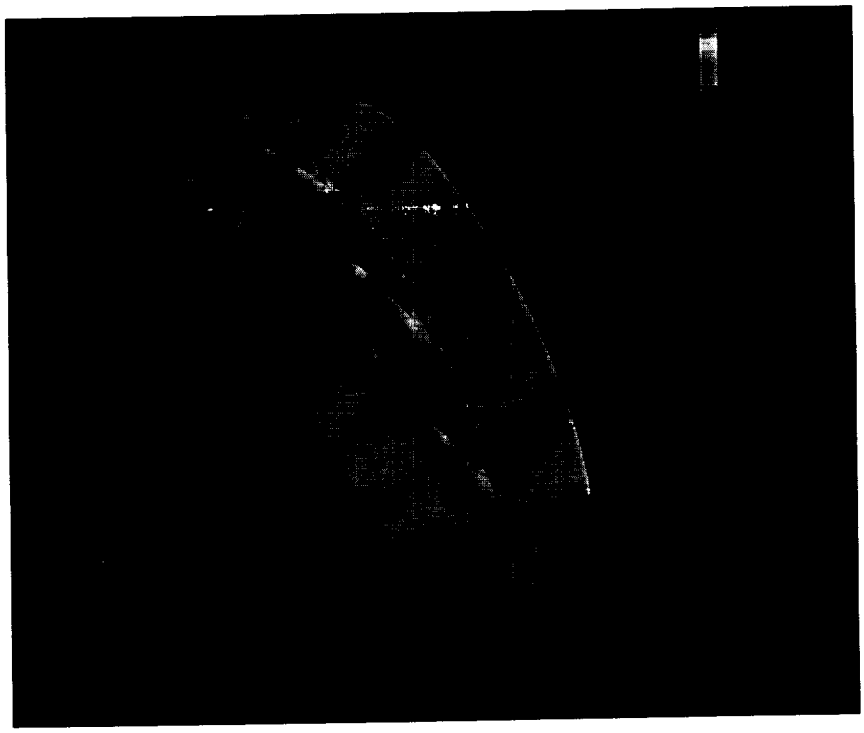

Figure 5. Instantaneous Mach contours - upstream view - partial admission.

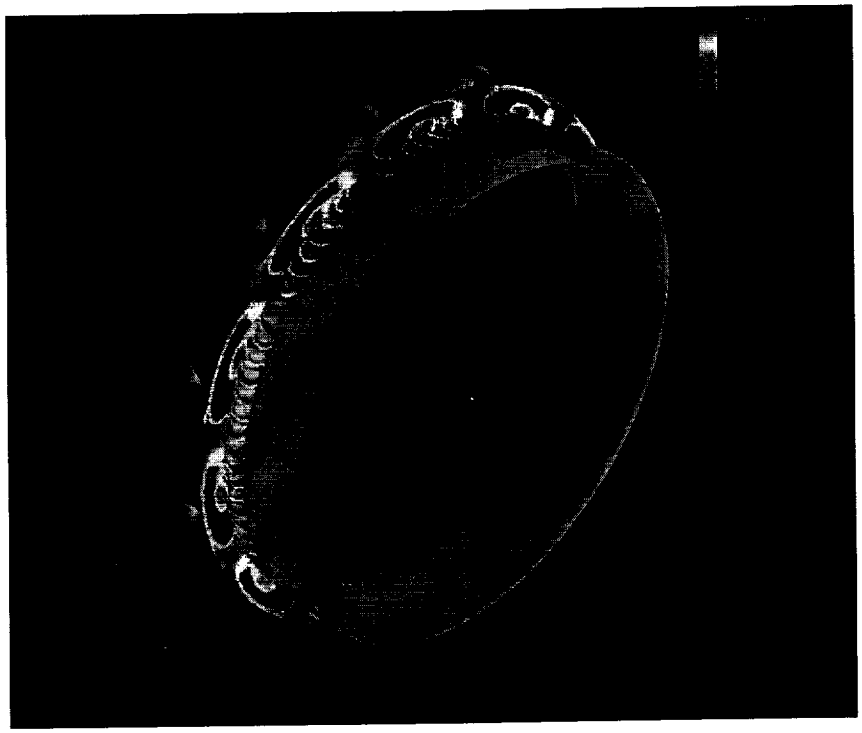

Figure 6. Instantaneous Mach contours - downstream view - full admission.

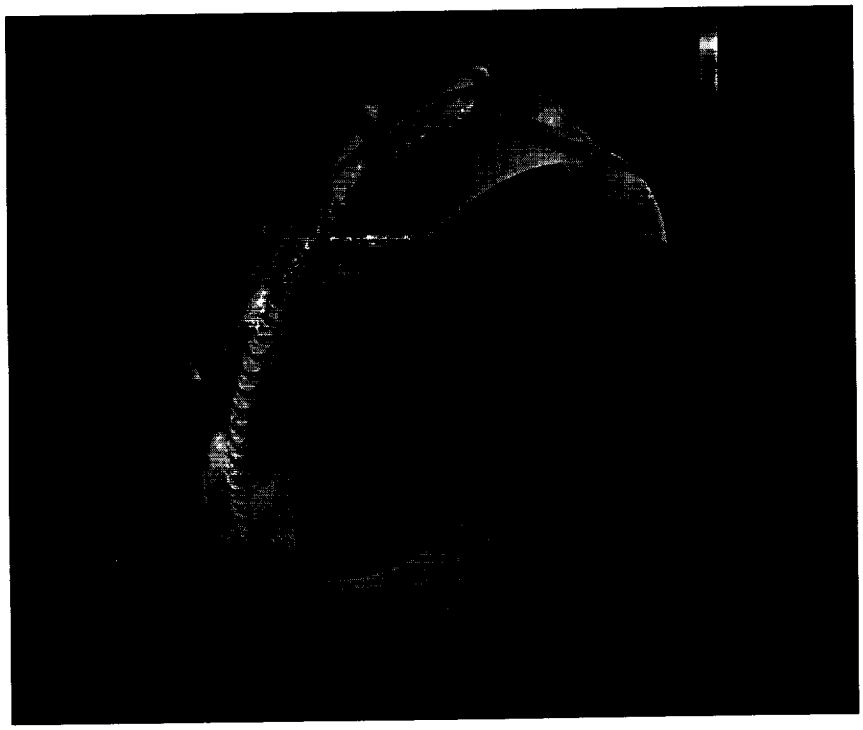

Figure 7. Instantaneous Mach contours - downstream view - partial admission.

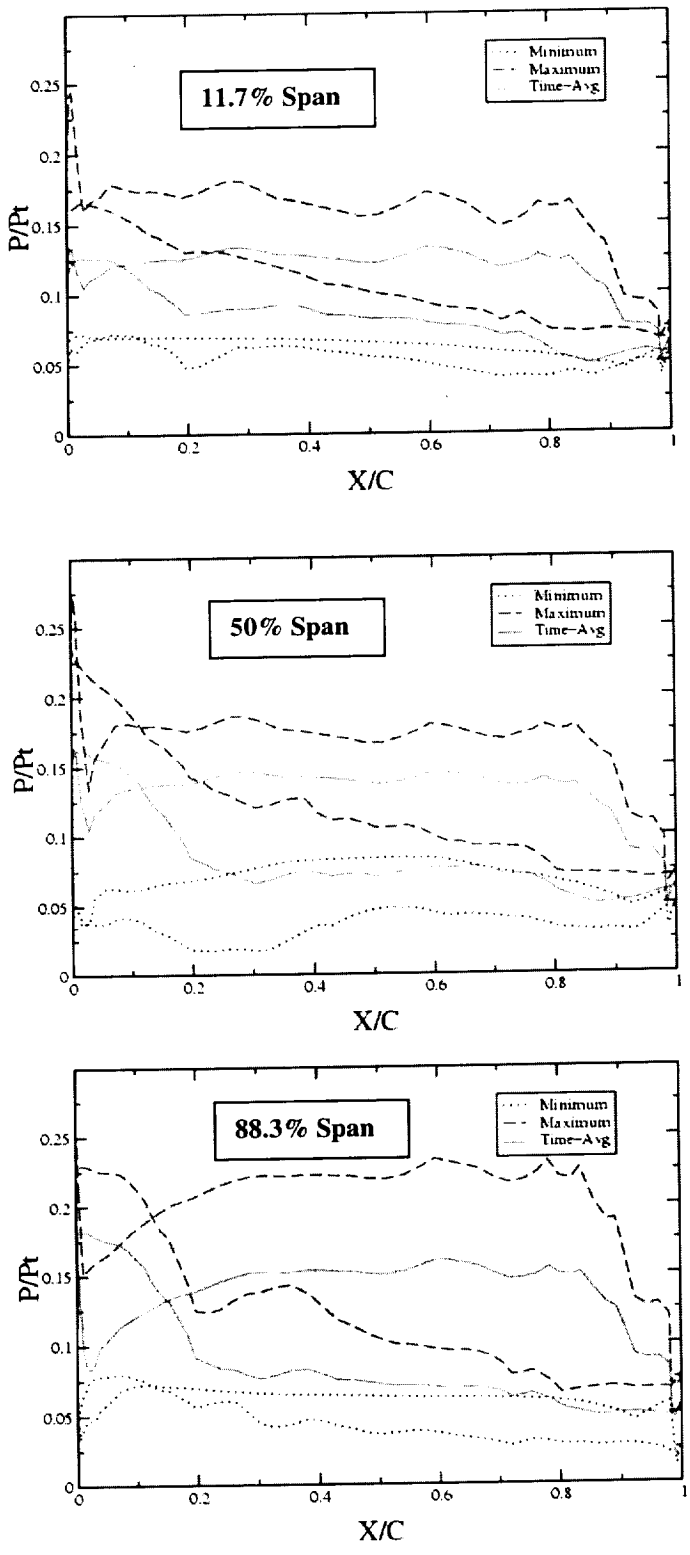

Figure 8. Rotor unsteady pressure envelopes - full admission.

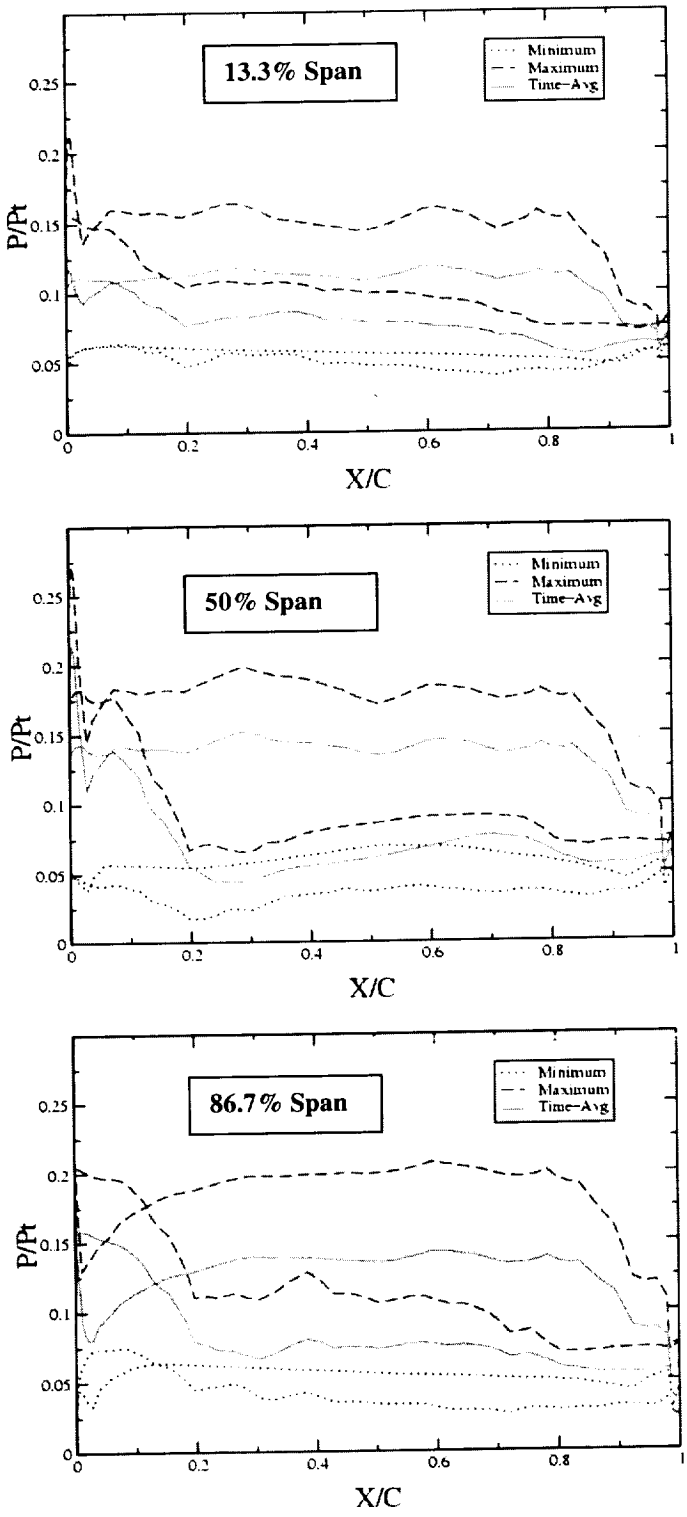

Figure 9. Rotor unsteady pressure envelopes - partial admission in nozzle jets.

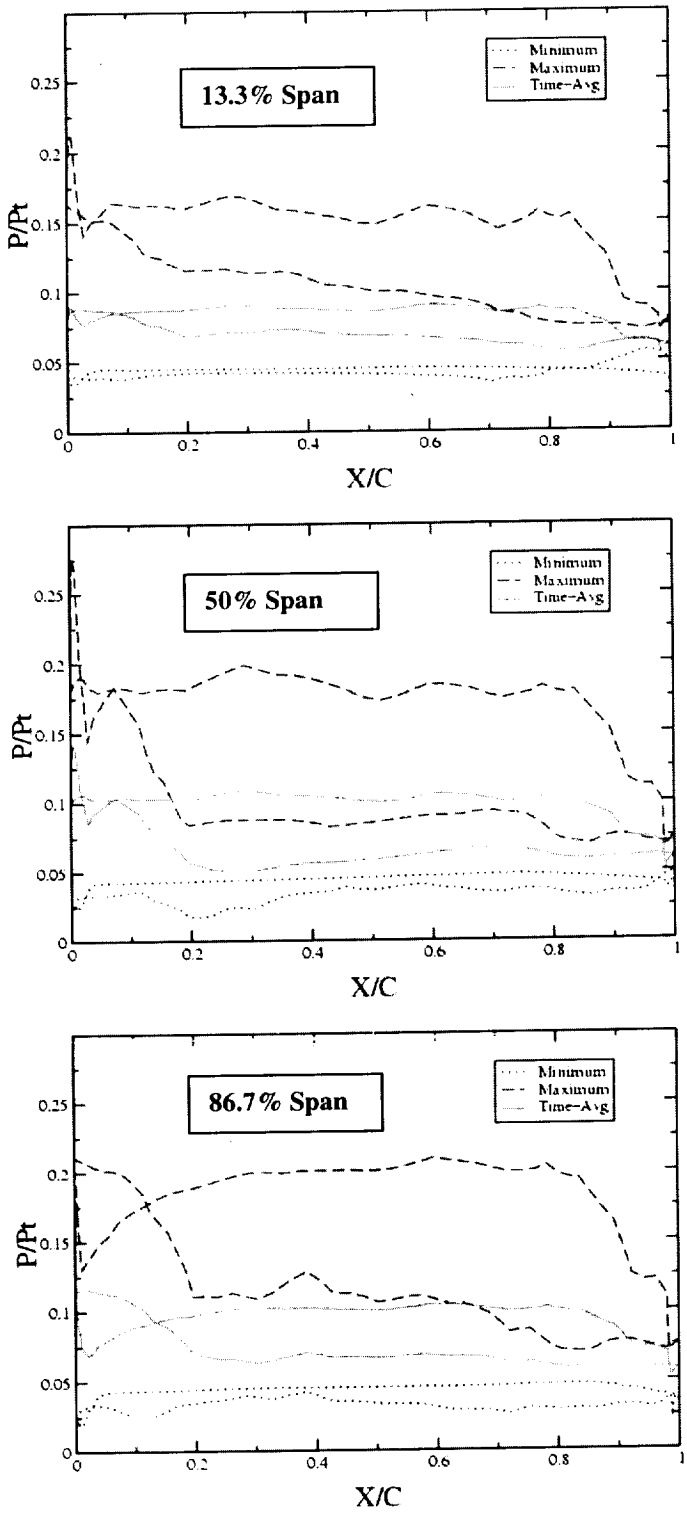

Figure 10. Rotor unsteady pressure envelopes - partial admission in all regions.

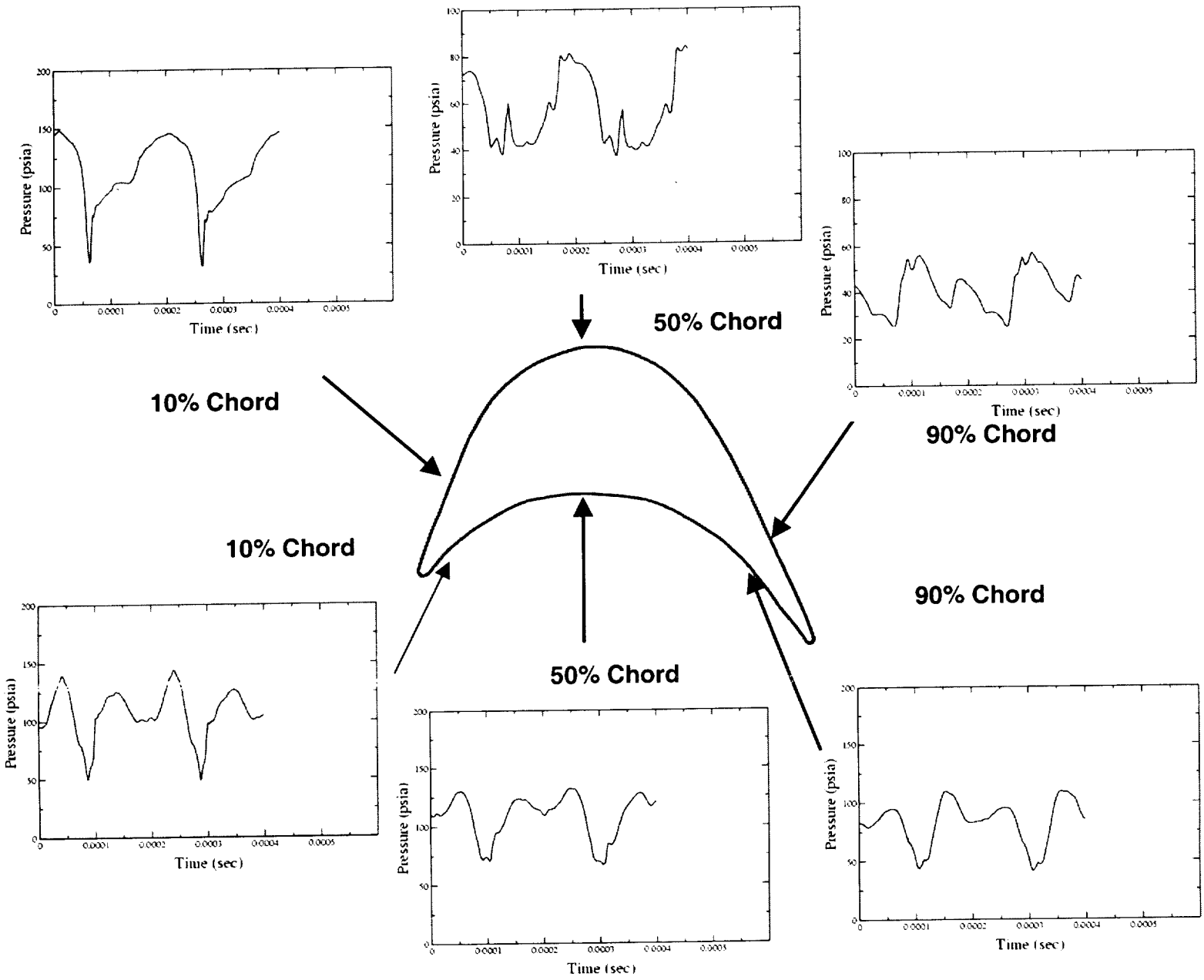

Figure 11. Unsteady pressure traces – full admission – 50% span.

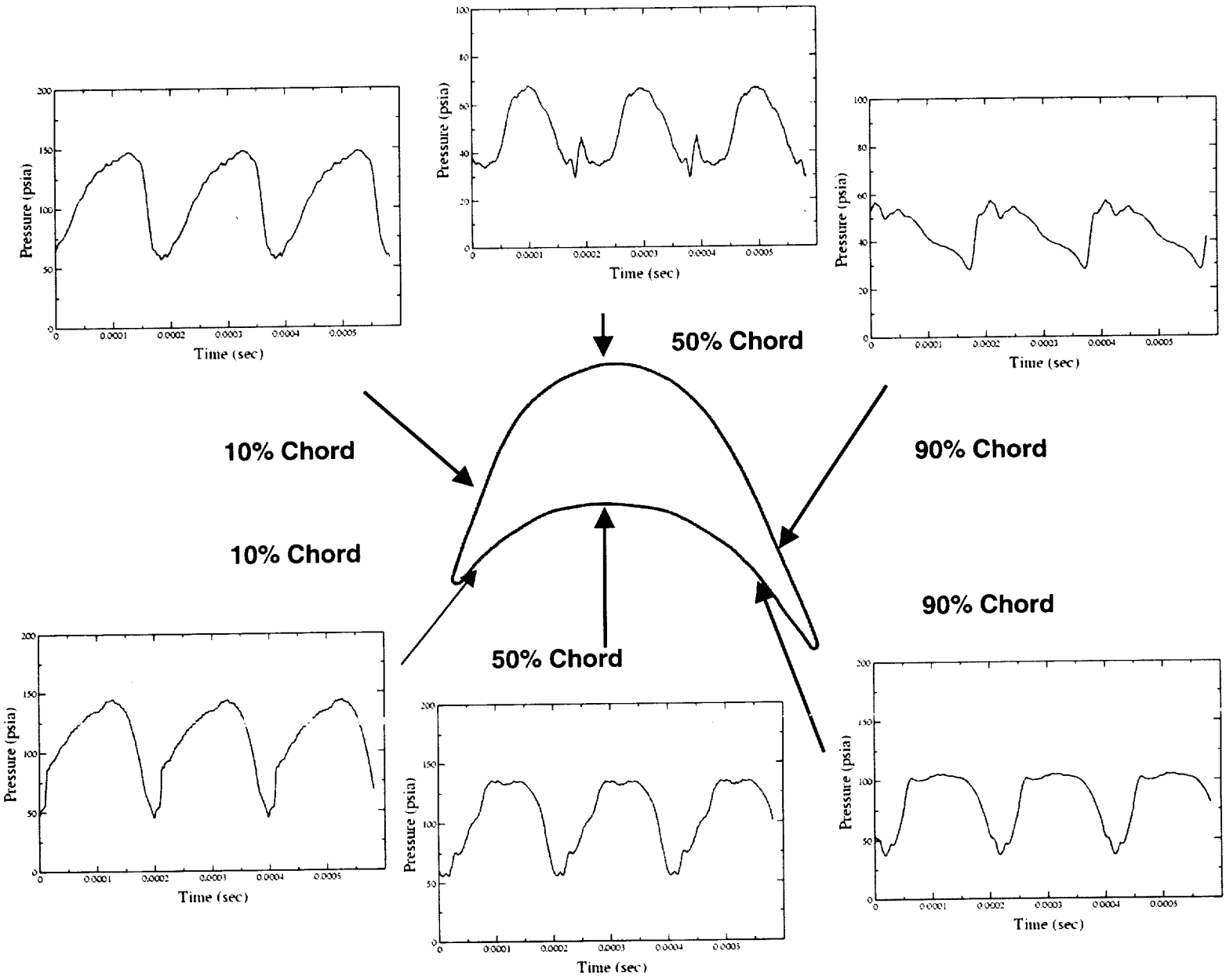

Figure 12. Unsteady pressure traces – partial-admission – 50% span – in nozzle jets.

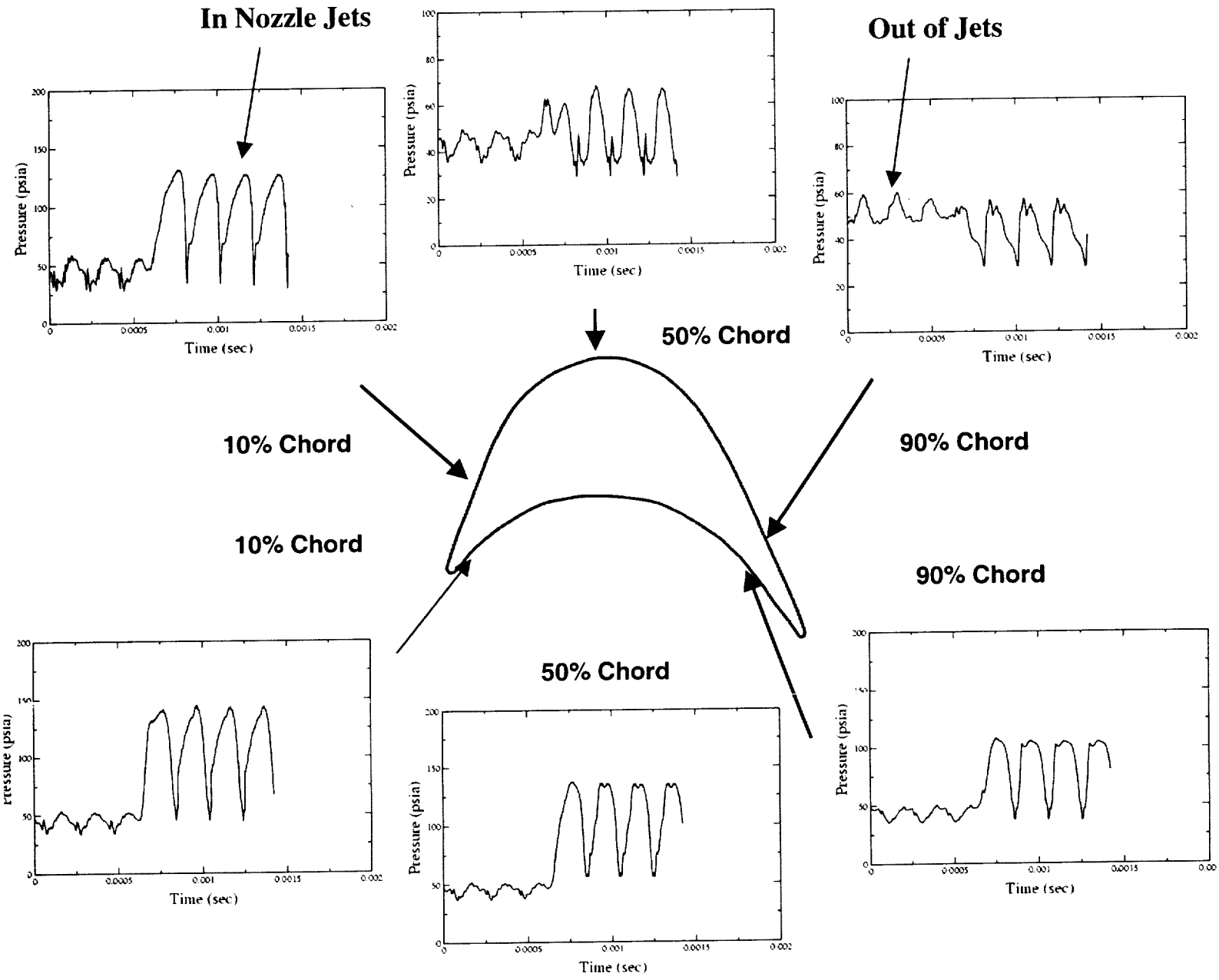

Figure 13. Unsteady pressure traces – partial-admission – 50% span – in and out of nozzle jets.

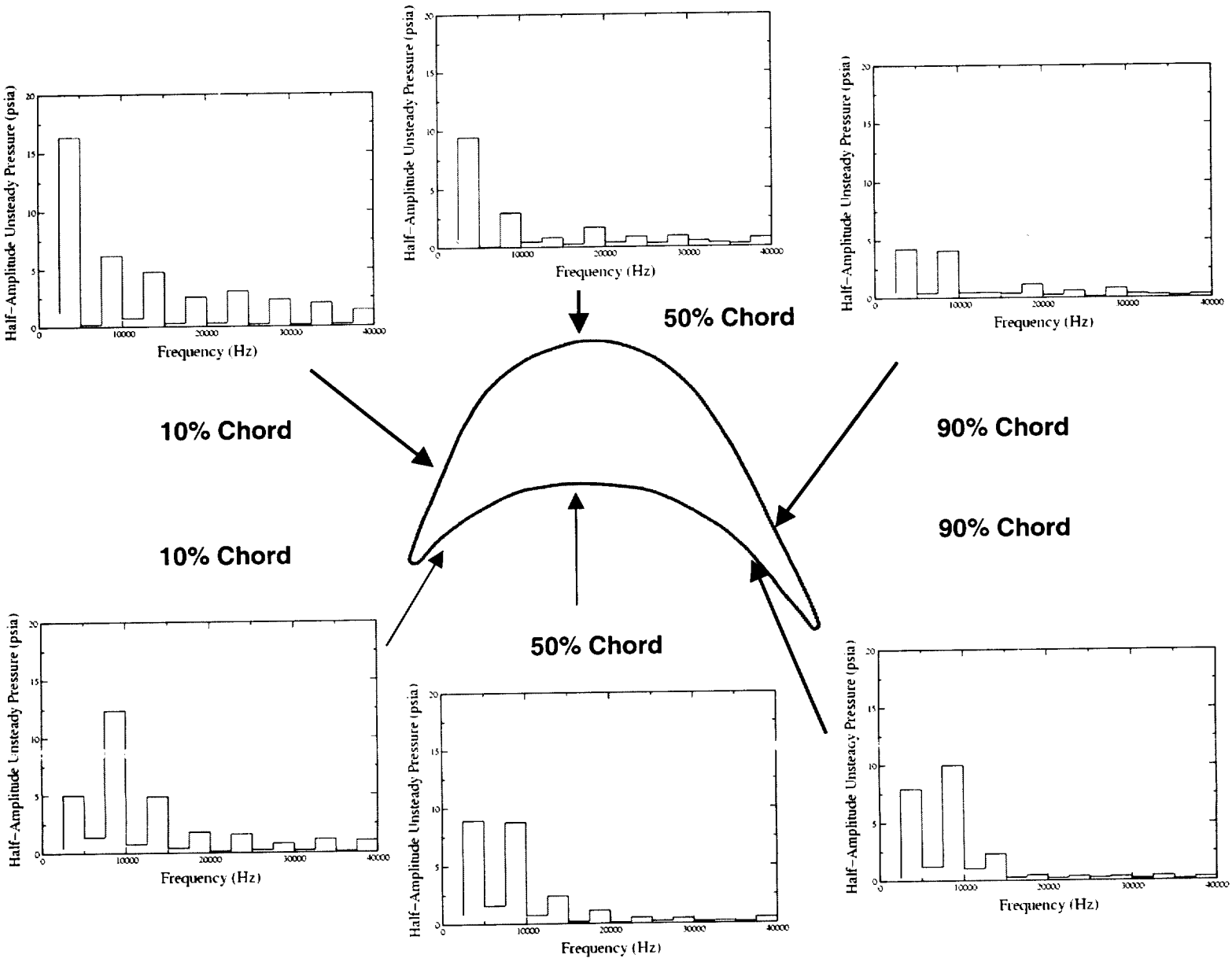

Figure 14. Decomposition of unsteady pressure – full-admission – 50% span .

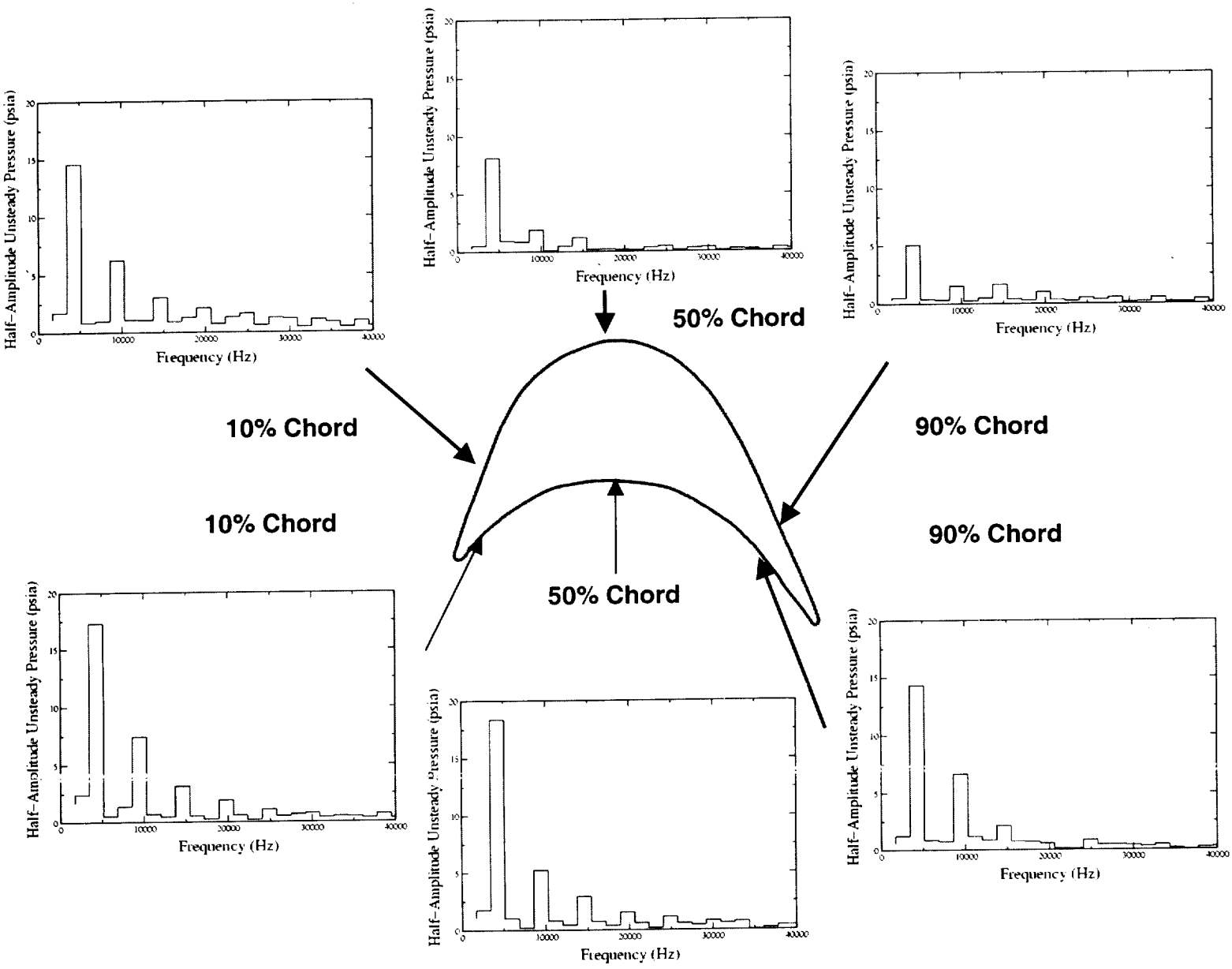

Figure 15. Decomposition of unsteady pressure – partial-admission – 50% span – in nozzle jets.

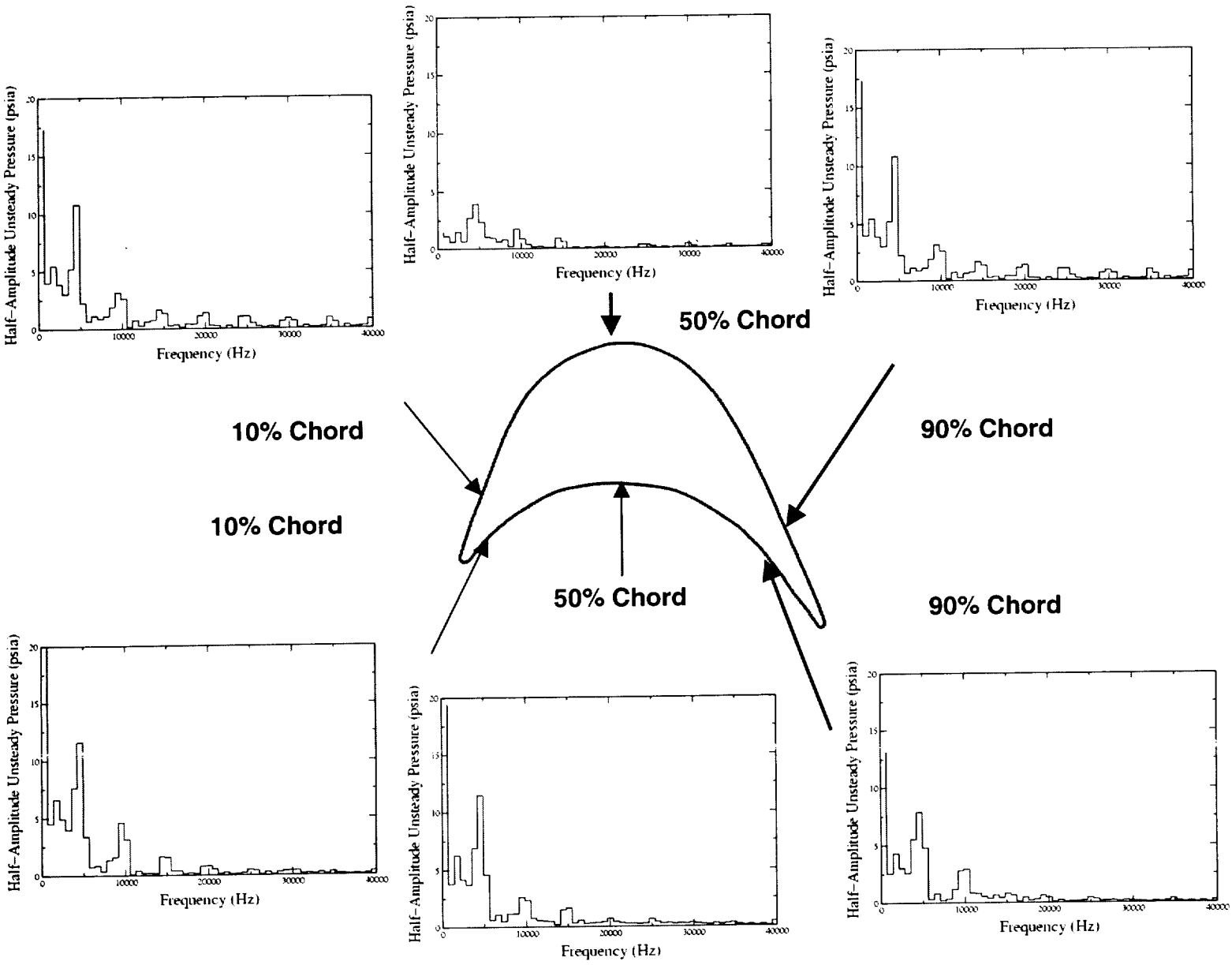

Figure 16. Decomposition of unsteady pressure – partial-admission – 50% span – in and out of jets.

Full Admission

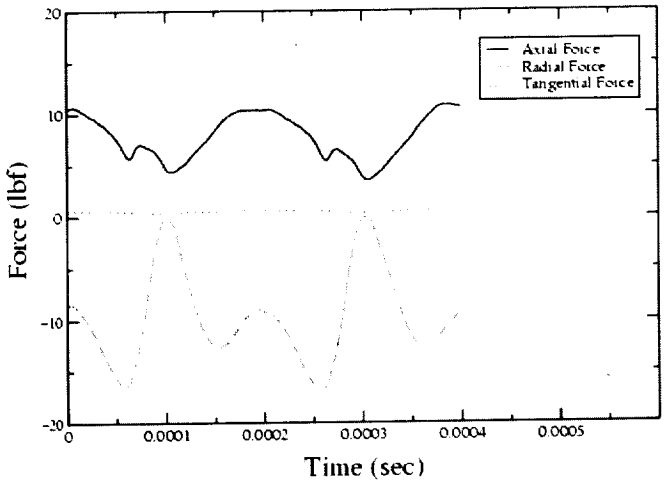

Partial Admission In Nozzle Jets

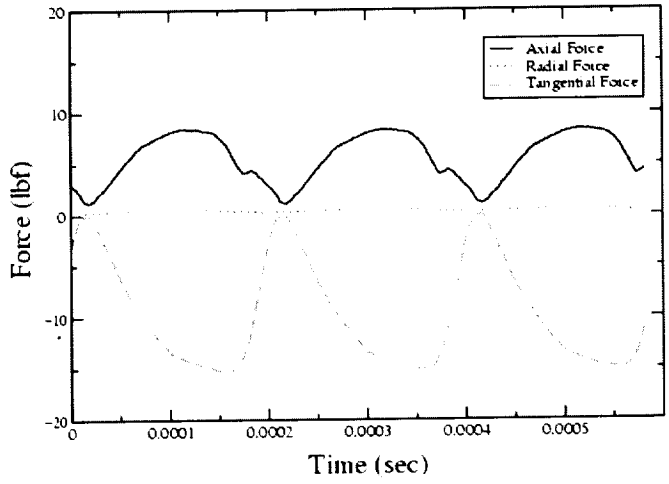

Partial Admission In/Out of Nozzle Jets

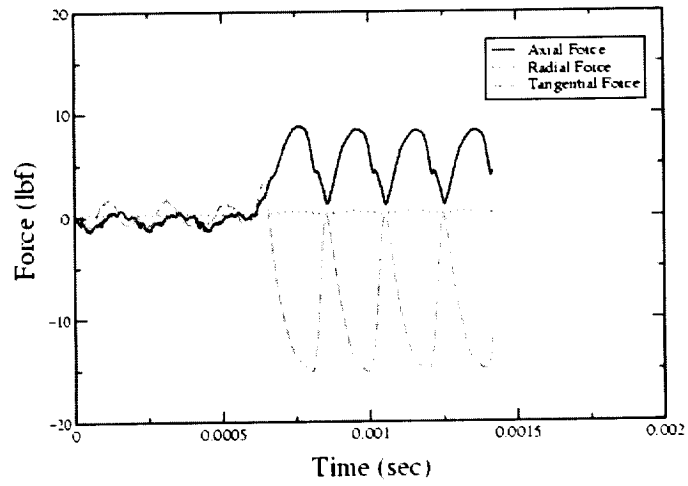

Figure 17. Unsteady forces.